Pergamon

0301-9322(95)00040-2

Int. J. Multiphase Flow Vol. 21, No. 6, pp. 1141–1161, 1995

0301-9322/95 $9.50 + 0.00

EXPERIMENTAL AND THEORETICAL STUDY OF THE DISTRIBUTION OF MASS CONCENTRATION OF SOLID PARTICLES IN THE TWO-PHASE LAMINAR BOUNDARY LAYER ON A FLAT PLATE

M. HUSSAINOV, A. KARTUSHINSKY†, A. MULGI, Ü. RUDI and S. TISLER

Department of Aeromechanics, Institute of Energy Research, Estonian Academy of Sciences, Paldiski Rd 1, EE0001 Tallinn, Estonia

(Received 25 January 1994; in revised form 26 April 1995)

Abstract—The essential non-uniform distribution of particle mass concentration, with vivid maximum value inside the two-phase laminar boundary layer developed in the flow past a flat plate, has been found by experimental investigation. The mathematical model based on the approximation of the dispersed phase within the viscous fluid, taking into consideration pseudoviscosity coefficients, has been elaborated for description of the motion and distribution of solid admixture. The dispersed phase is considered as a polydispersed phase, which consists of a finite number of particle fractions. The numerical results from the simplest version of the model are in good agreement with the experimental results, which indicates a principal possibility of applying the given mathematical model for flows of similar type.

Key Words: laminar boundary layer, self-similar co-ordinates, dispersed phase, particle mass concentration, interparticle collision, pseudoviscosity coefficients, particle fraction, particle angular momentum, restitution and friction coefficients

1. INTRODUCTION

A large number of manufacturing and natural processes are connected with the motion of particles in gas flows, e.g. combustion of solid fuels in thermal power stations, dust collection, pneumatic conveying and admixture diffusion in the atmosphere. The sedimentation of solid particles on streamlined surfaces can be included in these processes. The given investigation was carried out within the international project "Mars 94/96". The definition of the quantity of Martian dust sedimentation on the apparatus surfaces is of great importance in forecasting their security performance. One of the problems was to estimate the maximum possible value of particle sedimentation on the baloon surface. The sedimentation quantity was stipulated by particle motion near the streamlined surface. The laminar boundary layer was formed on the surface of the balloon while it was moving in the dusty Martian atmosphere. Thus, the object of the given investigation was to study the mechanism of particle motion and distribution inside the laminar boundary layer. Laminar flow past the unyawed flat plate by vertical two-phase flow for the Reynolds numbers 10^3–10^4 was considered. Knowing the distribution of particle mass concentration in such a two-phase laminar boundary layer, we can determine the sedimentation intensity of solid particles on the surface.

A suitable experimental rig has been built in our laboratory for investigating the motion of solid admixture in the vicinity of streamlining bodies. The measurements of relative particle mass concentration and velocities of both phases were carried out using laser diagnostics. Experimental investigations have essentially shown non-uniform distribution of particle mass concentration with the maximum value inside the boundary layer, which substantially differs from that obtained according to well-known theoretical conceptions (Soo 1971; Osyptsov 1981; Amsolov 1992). According to these conceptions, the maximum particle concentration is on the plate surface. The mathematical model, not considering the dispersed medium as an ideal gas, but as a Newtonian

†To whom all correspondence should be addressed.

viscous fluid and introducing pseudoviscosity coefficients, was elaborated for describing such a distribution of particle mass concentration. These pseudoviscosity coefficients are determined by the consideration of the interparticle collision mechanism and they characterize the diffusion of mass and the momentum of the dispersed phase. Since in manufacturing and in nature the composition of real powders are polydispersed and the particles have an irregular form, the assumption of monodispersity of the dispersed phase cannot adequately describe the motion of particles in various phenomena. Therefore, to describe the behaviour of the dispersed phase, it is necessary to take into account its real composition. The presented mathematical model considers the dispersed phase as polydispersed, consisting of a finite numer of particle fractions with different sizes. Since the particles of different sizes have different velocities along their paths, the interparticle collisions are taken into account. Simulation of specific boundary conditions on the surface and in the outer part of the boundary layer is a pecularity of the presented model. By applying such a method we can correctly describe the experimentally observed distribution of particle mass concentration near the surface.

2. EXPERIMENTAL STUDY

The experiments were carried out in a disconnected vertical two-phase wind-channel with an open working space (figure 1). The aerodynamical bench consisted of the following parts: a main channel for formation and transportation of two-phase flow; a channel of concurrent pure air flow; a device for formation of a flow field with the given parameters in the working space of the wind-channel; and a dust suck-out channel. Also, the aerodynamical bench included a blower, particle screw feeder, air flow governor, a thermocontroller, a particle screw feeder, a flowmeter, a pressure converter and optical registering, controlling and processing systems.

The wind-channel functioned by injecting a solid suspension into the open working space with given parameters and subsequent ejection through the diffuser. The two-phase flow was set up by forming a device consisting of a cylindrical tube with a diameter of 100 mm and length of 3 m. The tube was installed along the axis of the forming device. After exiting the cylindrical tube and passing

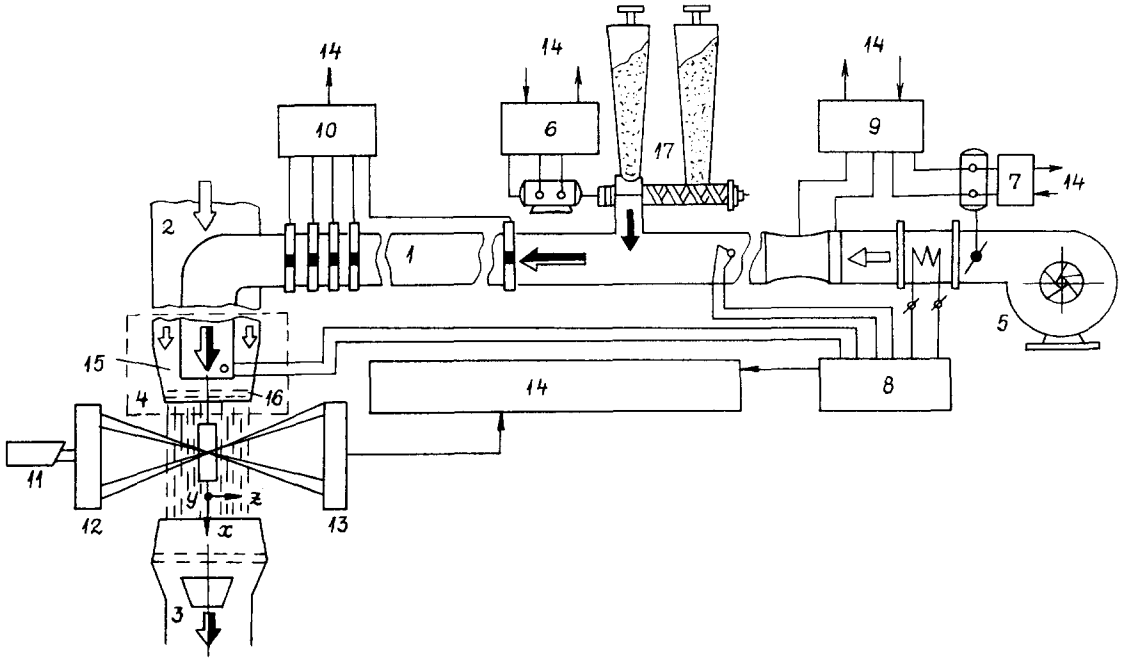

Figure 1. Aerodynamical bench: 1, main channel; 2, channel of concurrent pure air flux; 3, a dust suck-out channel; 4, a device for formation of the given flow field; 5, blower; 6, particle screw feeder; 7, air flow governor; 8, thermocontroller; 9, flowmeter; 10, pressure converter; 11 He–Ne laser; 12, transmitting optics; 13, receiving optics; 14, registering, processing and controlling system; 15, confuser; 16, system of grates; 17, particle screw feeder.

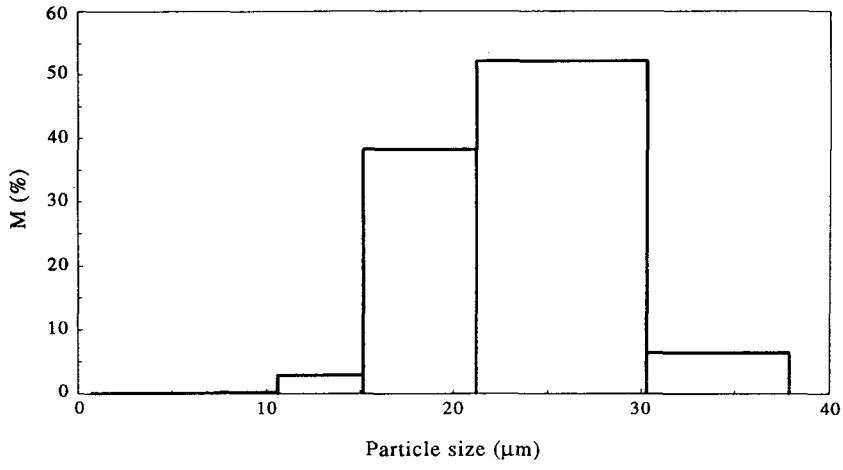

Figure 2. The particle mass distribution for the average particle diameter $\delta = 23\,\mu$m.

through the system of grates, the formed two-phase suspension expanded and entered the open working space supported by the concurrent flow of pure air on either side. Three grates, with mesh sizes of 0.63, 0.315 and 0.15 mm at an interval of 12 mm, were used for smoothing the parameters of inflow. The uniformity of the two-phase flow with the given parameters was obtained by varying the pure air flow in one of the channels, the two-phase flow in another and also in the dust suck-out channel.

The distributions of the local averaged parameters (velocity and particle mass concentration) of the two-phase flow in the vicinity of a flat plate were measured with the help of a forward-scatter laser Doppler anemometer (LDA) and laser concentration measurer (LCM) (He–Ne laser, sending and receiving optics in figure 1). The optical parts of the LDA and LCM have been installed on a special coordinate device controlled by a PC. This allowed scanning of the flow continuously or discretely in any given direction with an accuracy of 0.1 mm. The optical system included a 50 mW helium–neon laser. The LDA receiving optics contained two channels: one has been tuned for registering signals from small flow tracers and the second for measuring the dispersed phase. Each channel consisted of receiving optics, fiber cable, a photomultiplier (PM) and a special counter processor. Tuning of the channels was based on the amplitude discrimination of the Doppler signals. The channel of the dispersed phase has been tuned for registering signals only from the particles of this phase by selecting the geometry of reception and sensitivity of the PM. The measurements of particle mass concentrations were based on measuring the light intensity of the beam scattered at some angle and an attenuated direct beam in the optical heterogeneous medium.

Manufactured abrasive electrocorundum powders (Al_2O_3; $\rho_p = 3950\,\text{kg/m}^3$), while average particle sizes of 12, 23 and 32 μm, were used in the experiments. A large number of natural and manufactured dispersed abrasive materials have a granulous form and a high polydispersity, i.e. they contain particles with different sizes. Since the physical properties of the dispersed systems depend significantly on the fractional composition of the powders, it is necessary to know the particle size distributions and thus analysis of the polydispersity of the applied powders was made beforehand. The results of this analysis for the standard powder M28, as an example, are presented in figure 2 (here the mass content M of the given fraction is laid out along the ordinate and the lower and upper limits are given on the abscissa). A stainless steel flat plate was used as a model for investigations. It has the following dimensions: length 500 mm, width 100 mm, thickness 2 mm. The leading edge of the plate is wedge-shaped with a single bevel of the rear surface of the plate.

The model was installed into the uniform, completely formed, vertical, two-phase flow with the settled parameters. The distributions of gas velocity U_∞ and relative mass particle concentration α/α_∞ in the working space of the wind-channel are presented in figure 3 where $\alpha_\infty = \rho_{s\infty}/\rho$ and ρ, ρ_∞ are densities of the gas and dispersed phase in the stream flow, respectively. The diameter of the uniform flow in the working space was 150–180 mm depending on the stream velocity. The main parameters of the experiments (U_∞, δ, ρ_∞) were stipulated by the steady formation of the two-phase

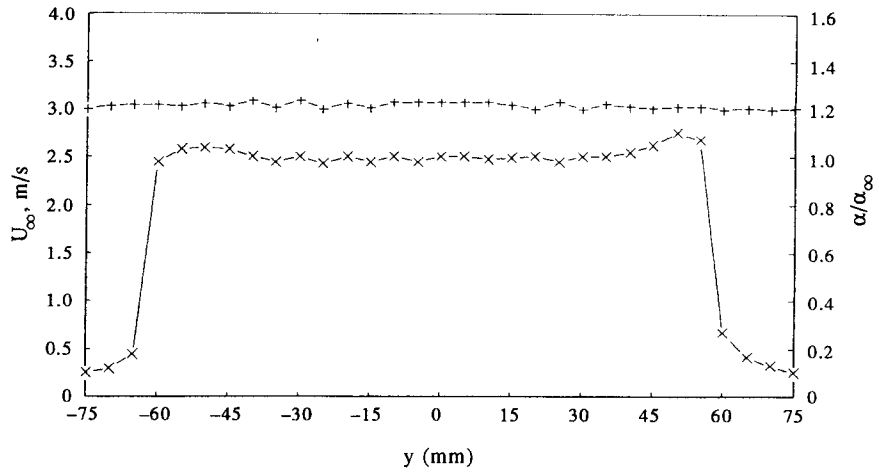

Figure 3. Profiles of the axial velocity component (−+−+−) and particle mass concentration (−×−×−) in the working space of the wind-channel.

laminar boundary layer on a plate and by uniform feeding of the dispersed phase into the working space of the wind-channel. The values of stream velocity were 1.5 and 3 m/s. The Reynolds number Re_x in the investigated cross-sections of the plate did not exceed 4×10^4. The concentration of solid admixture was due to the absence of feedback of the solid phase to the carrier flow ($\rho_\infty \ll 1$) and equalled $\rho_{s\infty} = 0.01$ kg/m^3.

The main error in the measurements of particle mass concentration in the boundary layer is stipulated by time instability and by the non-uniformity of the particle concentration over the cross-section of the stream flow. The non-uniformity of the particle mass concentration for various particle sizes is almost the same and does not exceed 5%. The time instability of the concentration is caused by functioning of the particle screw feeder and by particle sedimentation on the walls of the main channel of transportation of the two-phase flow and on the surfaces of the forming device. This instability became apparent only for 12 μm particles due to their high adhesiveness. The concentration profiles have been obtained by averaging data from more than 10 measuring series for every cross-section of the plate. Experimental uncertainties for particle mass concentration were as follows: for 12 μm particles < 15%; for 23 and 32 μm particles < 10%.

Profiles of the relative particle mass concentration in the two-phase laminar boundary layer on a flat plate in the cross-sections $X = 50$, 100 and 170 mm are pesented in figures 4 and 5. The experiments show that the given non-uniform concentration profiles have already been formed at

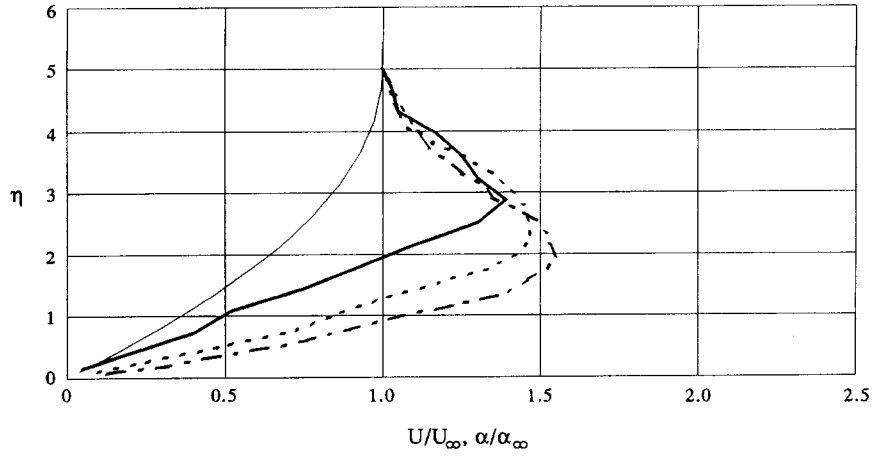

Figure 4. Experimental profiles of the axial velocity component of gas (——, U/U_∞) and particle mass concentration α/α_∞ for the free stream velocity $U_\infty = 1.5$ m/s and $\delta = 23$ μm: ——, $X = 50$ mm; -----, $X = 100$ mm; –·–·–, $X = 170$ mm.

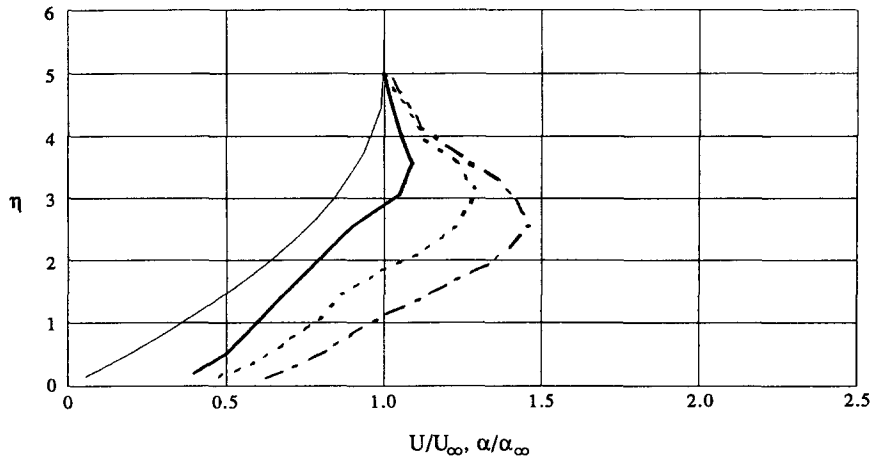

Figure 5. Experimental profiles of the axial velocity component of gas (——, U/U_∞) and particle mass concentration α/α_∞ for the free stream velocity $U_\infty = 3$ m/s and $\delta = 23\,\mu$m: ——, $X = 50$ mm; -----, $X = 100$ mm; – – – –, $X = 170$ mm.

the leading edge of a flat plate (at a distance of 10 mm from the leading edge) and remained almost the same downstream. As follows from these charts, the distribution of particle mass concentration reaches a maximum for both free stream velocities (1.5 and 3 m/s). The value of concentration maximum increases along the plate from the leading edge and holds downstream while its self-similar coordinate decreases. Figures 6 and 7 show the influence of particle size on the distribution of particle mass concentration. The distribution of particle mass concentration has a maximum for all the investigated particle sizes (12, 23 and 32 μm).

3. THEORETICAL MODEL

3.1. General remarks

The solid particle-laden laminar boundary layer, developed when flowing past an unyawed flat plate, is considered within the Eulerian approach where the dispersed phase is modelled as a continuous medium. The dispersed phase is described within mutually-penetrating continua by Nigmatulin's theory (1978), since the interparticle distance e is much smaller than the characteristic flow scale, which here is the thickness of the boundary layer Δ. This also emanates from the

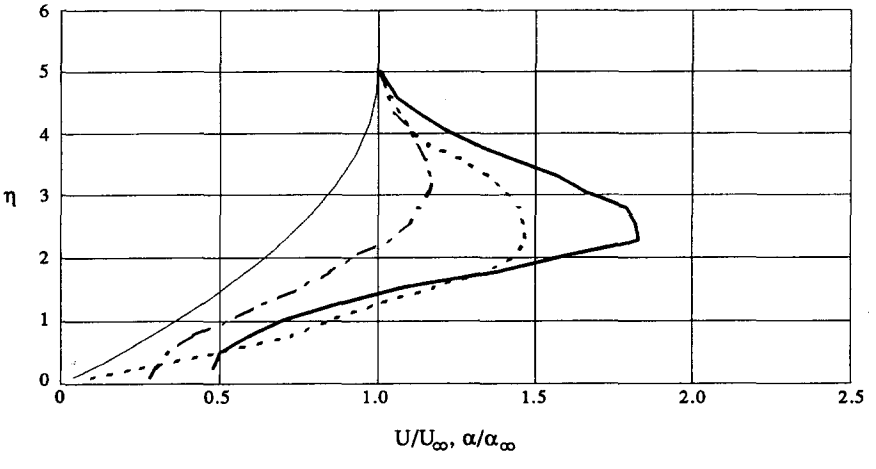

Figure 6. Experimental profiles of the axial velocity component of gas (——, U/U_∞) and particle mass concentration α/α_∞ for the free stream velocity $U_\infty = 1.5$ m/s and cross-section $X = 100$ mm: ——, $\delta = 12\,\mu$m; -----, $\delta = 23\,\mu$m; – – – –, $\delta = 32\,\mu$m

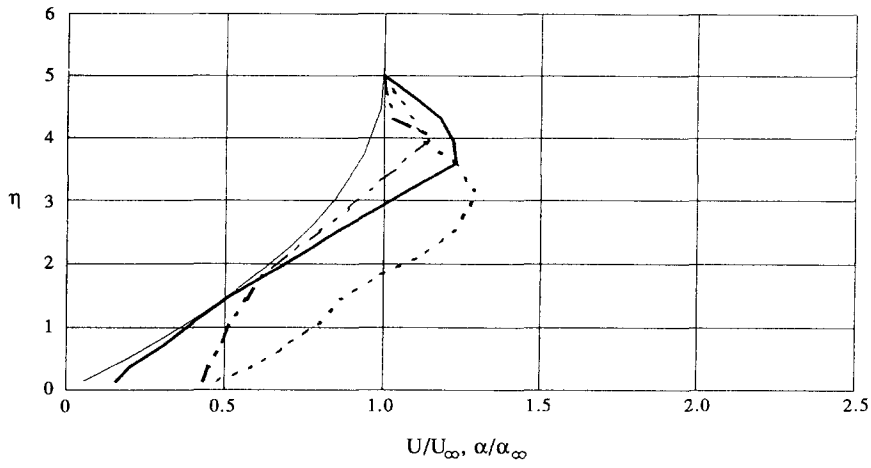

Figure 7. Experimental profiles of the axial velocity component of gas (——, U/U_∞) and particle mass concentration α/α_∞ for the free stream velocity $U_\infty = 3$ m/s and cross-section $X = 100$ mm: ——, $\delta = 12\,\mu$m; -----, $\delta = 23\,\mu$m; –·–·–, $\delta = 32\,\mu$m

necessity of theory validation. As our calculations show, e.g. for 10 μm particles with a particle mass concentration $\alpha_\infty = 0.01$, the ratio l/Δ is an order of $(l/\Delta) \approx O(10^{-1})$.

Unlike the approach of an ideal gas for description of the dispersed phase in a two-phase laminar boundary layer (Soo 1971; Osyptsov 1980; Asmolov 1992), the transport equations of particle mass, linear and angular momenta of the dispersed phase are written using the approximation of the Newtonian viscous fluid for that phase. Soo (1971), Osyptsov (1980) and Asmolov (1992) calculated the two-phase laminar boundary layer on a flat plate with monodispersed particles and, also, Asmolov (1992) took into account the influence of the Saffman force on the motion and distribution of the dispersed phase. Therefore they considered only the convectional transfer of the dispersed phase in the boundary layer. We account for, in addition to the convectional transfer and particle–gas and particle–wall interactions, the diffusion transfer of the particles, which is described by considering the interparticle collision mechanism. As a result of such a theoretical description, the pseudoviscosity coefficients of the dispersed phase ν_s^1, ν_s^2, $\nu_s^3 D_s$ are brought into consideration. Interparticle collision results from velocity differences of single partilces in the real two-phase flows. The differences in particle velocities in turn have been stipulated by the polydispersity of the real solid admixture content. As experimental data show, the content of the electrocorundum powder is non-uniform and the particles themselves have an irregular form. The particle mass distribution against the particle size is shown in figure 2 for the electrocorundum powder with a mean particle size $\delta = 23\,\mu$m. The root-mean-square deviation of particle sizes is up to 30%.

For the mathematical description of the solid admixture the real continuous particle size distribution is modelled by the finite number of particle fractions of discrete size. Each fraction is characterized by its own properties, such as particle size, concentration and velocity. This allows the collision process between particles having different velocities to be taken into consideration. We can write the transport equations and set the boundary conditions for each particle fraction. The correlations between the different particle fractions are calculated by introducing the pseuodviscosity coefficients derived from the collision mechanism.

We restrict our consideration by the description of two-dimensional motion of a two-phase flow in the laminar boundary layer. The composition of the polydispersed admixture is modelled by three fractions of particles: the fraction which contained the particles with the largest percent by mass (the so-called "main fraction" and denoted by index 2) and two additional particle fractions with smaller percents by mass. One of these additional fractions (index 1) consists of particles of a smaller size than the size of the particles from the main fraction. The other additional fraction (index 3) includes particles of a larger size in comparison with the particles from the main fraction. The dispersed phase is considered in the model as a polydispersed phase and is characterized by the following quantities: the particle sizes of the fractions $\delta_1 < \delta_2 < \delta_3$; velocity projections

$u_{s1}, v_{s1}, u_{s2}, v_{s2}, u_{s3}, v_{s3}$ in the streamwise and transversal directions, respectively; angular particle velocities $\omega_{s1}, \omega_{s2}, \omega_{s3}$ and particle mass concentration of the fractions $\alpha_1, \alpha_2, \alpha_3$.

The impact of the carrier fluid on the motion of the dispersed phase in the laminar boundary layer is realized via the drag force and two lift forces—those of Magnus & Saffman. The particles obtain their rotation by interaction with the surface of a plate. In addition to the transport equation of particle mass and the linear momentum of the dispersed phase, the transport equation of the angular momentum of particles is considered in the presented model. This equation is derived from the formula which describes the damping of the angular velocity of a single particle in the viscous medium (Rubinow & Keller 1965). By applying the spatial averaging method (Nigmatulin 1978) to this equation and to the equations of the translational motion of a single particle, we obtain the equations for describing the dispersed phase as a continuum. There is a prerequisite for the action of the Saffman force in the laminar boundary layer, since the parameter $u/\sqrt{v(\partial u/\partial y)}$ (Saffman 1961) is of a unit value unlike in the turbulent boundary layer, where it is much higher than a unit. Here u is the streamwise velocity component of gas and v is the laminar viscosity of gas. The gravity force is neglected due to the insignificance of the particle settling velocity relative to the particle velocity originating from the drag force. Other force factors (the Basset force, the force of added masses) have also been neglected, since the ratio of particle material density to the gas density is very high.

3.2. The equations and boundary conditions

Let us consider the two-dimensional motion of both phases in the laminar boundary layer. The equations of the two-phase laminar boundary layer in the Cartesian coordinate system are:

$$\frac{\partial \rho u}{\partial x} + \frac{\partial \rho v}{\partial y} = 0, \qquad [1]$$

$$\rho u \frac{\partial u}{\partial x} + \rho v \frac{\partial u}{\partial y} = \frac{\partial \tau}{\partial y}, \qquad [2]$$

$$\frac{\partial (\rho_s u_s)}{\partial x} + \frac{\partial (\rho_s v_s)}{\partial y} = \frac{\partial}{\partial y}\left(D_s \frac{\partial \rho_s}{\partial y}\right), \qquad [3]$$

$$\rho_s u_s \frac{\partial u_s}{\partial x} + \rho_s v_s \frac{\partial u_s}{\partial y} = \frac{\partial \tau_s}{\partial y} + \frac{\rho_s}{\rho_p}\left[\frac{18 C'_D v(u - u_s)}{\delta^2} + \frac{3}{4}(v - v_s)\left(\omega_s - \frac{\partial u}{2\partial y}\right)\right], \qquad [4]$$

$$\rho_s u_s \frac{\partial v_s}{\partial x} + \rho_s v_s \frac{\partial v_s}{\partial y} = \frac{\partial p_s}{\partial y} + \frac{\rho_s}{\rho_p}\left[\frac{18 C'_D v(v - v_s)}{\delta^2} + \frac{3}{4}(u - u_s)\left(\omega_s - \frac{\partial u}{2\partial y}\right) + \frac{6 \cdot K_s \sqrt{v}}{\pi \delta}(u - u_s)\sqrt{\frac{\partial u}{\partial y}}\right], \qquad [5]$$

$$\rho_s u_s \frac{\partial \omega_s}{\partial x} + \rho_s v_s \frac{\partial \omega_s}{\partial y} = -\frac{\partial \rho_s \langle \omega_s v_{sd} \rangle}{\partial y} - \frac{60 \rho_s v}{\rho_p \delta^2}\left(\omega_s - \frac{\partial u}{2\partial y}\right), \qquad [6]$$

where v is the transversal gas velocity component and v_{sd} is the particle diffusion velocity and ρ and ρ_p are the gas and particle material densities, respectively. The drag coefficient C'_D for different Reynolds numbers of a particle $\mathrm{Re}_p = \delta\sqrt{(u - u_s)^2 + (v - v_s)^2}/v$ is determined according to Kravtsov (1968) by the formula

$$C'_D = \frac{24}{\mathrm{Re}_p} = 1 + 0.275\sqrt{\mathrm{Re}_p} + 0.0138\ \mathrm{Re}_p. \qquad [7]$$

The density of the dispersed phase ρ_s is related to the density of incompressible gas ρ by $\rho_s = \alpha\rho$, which is valid if the volumetric concentration of particles is very low, i.e. $\beta \ll 1$. τ, τ_s are the shear stresses of the gas and dispersed phases, respectively, and p_s is the normal stress for the dispersed phase. $K_s = 1.61$ is the numerical constant (Shraiber *et al.* 1980).

We suggest that the behaviour of the dispersed phase obeys the approximation of the Newtonian fluid. Therefore, analogously to the gaseous carrier fluid the stress tensor components of the dispersed phase are correlated with the rate of strain via the introduced pseudoviscosity coefficients,

which can be written in the simplest form using the approximation of laminar boundary layer (Schlichting 1974):

$$\tau = \rho\nu \frac{\partial u}{\partial y}, \qquad [8]$$

$$\tau_s = \rho_s \nu_s^1 \frac{\partial u_s}{\partial y}, \qquad [9]$$

$$p_s = 2\rho_s \nu_s^2 \frac{\partial v_s}{\partial y}. \qquad [10]$$

We consider that the cross-product term $\langle \omega_s v_{sd} \rangle$ in [6], describing the transport of particle rotation, can be analogously obtained by using the approach of the mixing-length theory according to Tennekes & Lumley (1972). Introducing the pseudoviscosity coefficients ν_s^2, we can write:

$$\rho_s \langle \omega_s v_{sd} \rangle = -\rho_s \nu_s^3 \frac{\partial \omega_s}{\partial y}, \qquad [11]$$

where $\langle \cdots \rangle$ and further means an ensemble average. We also assume that the diffusive flow rate of particle mass is determined via the gradient of the concentration and pseudoviscosity coefficients analogously to the procedure for the molecular diffusion of gases.

The pseudoviscosity coefficients for the particle mass transport equation, for the momentum balance in streamwise and transversal directions and for the angular momentum balance of the dispersed phase are D_s, ν_s^1, ν_s^2, ν_s^3, respectively. These coefficients describe the transfer of mass, momentum and angular momentum of the dispersed phase by the diffusion process (originating from the interparticle collisions). This transfer is considered in addition to convectional transfer and the interphase momentum exchange, which is caused by various forces (the viscous drag force, the Saffman and Magnus lift forces). The pseudoviscosity coefficients are varied both over the width and length of the boundary layer. As the calculations show, the values of these coefficients at the leading edge of the plate, where the distribution of velocity of the dispersed phase changes from uniform in the free stream flow to typical in the boundary layer, are comparable with the value of coefficient of laminar viscosity of the carrier fluid.

These transport equations are the continuity equation [1] and the momentum balance of gas [2], the transport equation of particle mass [3], the momentum balance of dispersed phase in streamwise and transversal directions [4] and [5], respectively and the transport equation of angular momentum [6] of the dispersed phase. The equations are obtained by applying Nigmatulin's theory of mutually-penetrating continua. On the right-hand side of the equations of the momentum balance of the dispersed phase in the streamwise [4] and transversal directions [5], the drag force and Magnus and Saffman lift forces are taken into account. We write transport equations for each particle fraction denoted by the index "i". The pseudoviscosity coefficients ν_{si}^i, D_{si} for each particle fraction can be determined by knowing the velocity and mass concentration fields of interacting fractions, i.e. u_{si}, v_{si}, ω_{si}, α_i. We consider one-way coupling because of the small particle mass loading (0.01 kg dust/kg air).

For transformation of the equations to the new coordinate system with the self-similar variables $x = x$, $\eta = y\sqrt{U/\nu x}$, i.e. using transformation as in the work by Anderson *et al.* (1990), let us write [1]–[6] with [8]–[11] in the following form:

$$x\frac{\partial \bar{U}}{\partial x} - \frac{\eta}{2}\frac{\partial \bar{U}}{\partial \eta} + \frac{\partial \bar{V}}{\partial \eta} = 0, \qquad [12]$$

$$x\bar{U}\frac{\partial \bar{U}}{\partial x} + \left[\bar{V} - \frac{\eta \bar{U}}{2}\right]\frac{\partial \bar{U}}{\partial \eta} = \frac{\partial^2 \bar{U}}{\partial \eta^2}, \qquad [13]$$

$$\sqrt{x}\frac{\partial}{\partial x}[\sqrt{x}\bar{\alpha}_i \bar{U}_{si}] + \frac{\partial}{\partial \eta}\left[\bar{\alpha}_i\left(\bar{V}_{si} - \frac{\eta \bar{U}_{si}}{2}\right)\right] = \frac{\partial}{\partial \eta}\left[\frac{D_{si}}{\nu}\frac{\partial \bar{\alpha}_i}{\partial \eta}\right], \qquad [14]$$

$$x\bar{U}_{si}\frac{\partial \bar{U}_{si}}{\partial x}+\left[\bar{V}_{si}-\frac{\eta \bar{U}_{si}}{2}\right]\frac{\partial \bar{U}_{si}}{\partial \eta}=\frac{\partial}{\partial \eta}\left[\frac{\nu_{si}^{1}}{\nu}\frac{\partial \bar{U}_{si}}{\partial \eta}\right]+\frac{\rho}{\rho_{p}}\frac{x}{\delta_{i}}\left[\frac{18C'_{Di}(\bar{U}-\bar{U}_{si})}{\mathrm{Re}_{pi}}\right.$$
$$\left.+\frac{3(\bar{V}-\bar{V}_{si})}{4\sqrt{\mathrm{Re}_{x}}}\left(\bar{\omega}_{si}-\frac{\mathrm{Re}_{pi}}{4\sqrt{\mathrm{Re}_{x}}}\frac{\partial \bar{U}}{\partial \eta}\right)\right], \quad [15]$$

$$x\bar{U}_{si}\frac{\partial \bar{V}_{si}}{\partial x}+\left[\bar{V}_{si}-\frac{\eta \bar{U}_{si}}{2}\right]\frac{\partial \bar{V}_{si}}{\partial \eta}=\frac{\partial}{\partial \eta}\left[\frac{2\nu_{si}^{2}}{\nu}\frac{\partial \bar{V}_{si}}{\partial \eta}\right]+\frac{\rho}{\rho_{p}}\frac{x}{\delta_{i}}\left[\frac{18C'_{Di}(\bar{V}-\bar{V}_{si})}{\mathrm{Re}_{pi}}\right.$$
$$\left.+\frac{3}{2}\sqrt{\mathrm{Re}_{x}}(\bar{U}-\bar{U}_{si})\left(\bar{\omega}_{si}-\frac{\mathrm{Re}_{pi}}{4\sqrt{\mathrm{Re}_{x}}}\right)+\frac{6\cdot K_{s}}{\pi}\frac{(\bar{U}-\bar{U}_{si})}{4\sqrt{\mathrm{Re}_{x}}}\sqrt{\frac{\partial \bar{U}}{\partial \eta}}\right]+\frac{\bar{U}_{si}\bar{V}_{si}}{2}, \quad [16]$$

$$x\bar{U}_{si}\frac{\partial \bar{\omega}_{si}}{\partial x}+\left[\bar{V}_{si}-\frac{\eta \bar{U}_{si}}{2}\right]\frac{\partial \bar{\omega}_{si}}{\partial \eta}=\frac{\partial}{\partial \eta}\left[\frac{\nu_{si}^{3}}{\nu}\frac{\partial \bar{\omega}_{si}}{\partial \eta}\right]-\frac{60\rho}{\rho_{p}\,\mathrm{Re}_{pi}}\frac{x}{\delta_{i}}\left[\bar{\omega}_{si}-\frac{\mathrm{Re}_{pi}}{4\sqrt{\mathrm{Re}_{x}}}\frac{\partial \bar{U}}{\partial \eta}\right], \quad [17]$$

where $\bar{U}=u/U_{\infty}$, $\bar{U}_{si}=u_{si}/U_{\infty}$, $\bar{V}=v\sqrt{x/\nu U_{\infty}}$, $\bar{V}_{si}=v_{si}\sqrt{x/\nu U_{\infty}}$, $\bar{\omega}_{si}=\omega_{si}\delta_{i}/2U_{\infty}$, $\bar{\alpha}_{i}=\alpha_{i}/\alpha_{\infty}$ are non-dimensional stretched variables, the local Reynolds number $\mathrm{Re}_{x}=U_{\infty}x/\nu$, the Reynolds number of particles for different fraction $\mathrm{Re}_{pi}=U_{\infty}\delta_{i}\sqrt{(\bar{U}-\bar{U}_{si})^{2}+(\bar{V}-\bar{V}_{si})^{2}}/\nu$ and U_{∞}, α_{∞} are the velocity and particle mass concentration of free stream, respectively.

One can see that the equations of the two-phase laminar boundary layer include non-self-similar terms, which depend on the axial (streamwise) coordinate "x". They characterize the influence of the force factors in the equations of momentum balance and angular momentum balance of the dispersed phase. One can also see that, as far as the axial coordinate extends, the ratio δ_{i}'/x decreases resulting in the reduction of the influence of force terms. The first terms on the right-hand side of the equations of particle mass transfer [14], momentum transfer in axial [15] and transversal directions [16] and angular momentum transfer [17] describe the diffusion of mass, momentum and angular momentum of different fractions and are determined via the introduced pseudoviscosity coefficients of the dispersed phase ν_{s}^{1}, ν_{s}^{2}, ν_{s}^{3}, D_{s}. The tems in square brackets on the right-hand side of the equations of momentum balance, [15] and[16], characterize the impact of the drag force and the Magnus and Saffman lift forces, respectively. The fourth term takes into accocunt the influence of the Saffman force and the last term on the right-hand side of [16] is a sequence of the transform of equations into a new self-similar coordinate system. The second term on the right-hand side of the equation of angular momentum balance of the dispersed phase [17] reflects decaying of the rotation of solid particles in the viscous medium.

3.3. The initial and boundary conditions

Since one-way coupling is considered in the given model and, hence, the non-self-similar terms (the force factors) on the right-hand side of [12] and [13] are absent, we have self-similar velocity distribution of gas in the new coordinates x, η. This solution results from the joint decision of [12] and [13] for $x=0$. The initial fields of axial velocity components of the solid phase of different fractions and particle mass concentrations are set as uniform distributions in the cross-section of the boundary layer:

$$\bar{U}_{si}=1, \quad [18]$$

$$\bar{\alpha}_{1}=\bar{\alpha}_{3}=0.2, \quad \bar{\alpha}_{2}=0.6, \quad [19]$$

where $\bar{\alpha}_{2}$ is the initial value of relative particle mass concentration for the main particle fraction, $\bar{\alpha}_{1}$ and $\bar{\alpha}_{3}$ are the initial values of relative particle mass concentration for other particle fractions.

The distribution of transversal velocity components of the dispersd phase at $x=0$ is set as:

$$\bar{V}_{si}=0. \quad [20]$$

The initial fields of angular velocity of different particle fractions are set uniform in the cross-section of the boundary layer and their values are obtained using the formula from Babukha & Shraiber (1972):

$$\bar{\omega}_{si} = (1 - k_t)\bar{U}_{si}. \quad [21]$$

Thus, the solid particles entering the boundary layer collide with the plate surface and obtain rotation due to the roughness of the plate surface. The rotation of particles depends also on the friction coefficient k_t (in calculations $k_t = 0.75$), which can be varied, in general, according to Bubukha & Shraiber (1972) in the range $-1 \leqslant k_t \leqslant 1$.

We set the boundary conditions for the equations of the gaseous phase as sticking and impenetrability conditions at the surface:

$$\bar{U}|_w = 0, \quad [22]$$

$$\bar{V}|_w = 0. \quad [23]$$

At the outer part of the boundary layer we set the axial velocity component of gas equal to the velocity in free stream and the gradient of the transversal velocity equal to zero:

$$\bar{U}|_\infty = 1, \quad [24]$$

$$\left.\frac{\partial \bar{V}}{\partial \eta}\right|_\infty = 0. \quad [25]$$

The boundary conditions for the equations of the dispersed phase, i.e. for the equations of the streamwise particle velocity component and the particle angular velocity, are set assuming the relative particle velocity along the surface as in the theory of rarefied gases (Chapman & Cowling 1960). The given expressions include the recovery coefficients of linear and angular momenta of particles at the interaction with the surface:

$$\bar{U}_{si}|_w = \gamma_u \left.\frac{\partial \bar{U}_{si}}{\partial \eta}\right|_w, \quad [26]$$

$$\bar{\omega}_{si}|_w = \gamma_\omega \left.\frac{\partial \bar{\omega}_{si}}{\partial \eta}\right|_w, \quad [27]$$

where the recovery coefficients γ_u, γ_ω, according to Chapman & Cowling (1960), are determined as:

$$\gamma_u = \frac{(l - f_u)}{f_u} l, \quad [28a]$$

$$\gamma_\omega = \frac{(2 - f_\omega)}{f_\omega} l. \quad [28b]$$

The formulae for f_u and f_ω are obtained using the results of Babukha & Shraiber (1972). Then one can write:

$$f_u = \frac{(5 + 2k_t)}{7}, \quad [29a]$$

$$f_\omega = \frac{(2 + 5k_t)}{7}. \quad [29b]$$

The friction coefficient k_t introduced by Babukha & Shraiber (1972) neglects the relative velocity of particles along the surface and thus differs from those introduced by Matsumoto & Saito (1970), who considered two types of particle–wall interaction—with and without relative velocity along the surface.

For the transversal velocity component of the dispersed phase the impenetrability conditions at the surface for each particle fraction are set as:

$$\bar{V}_{si}|_w = 0. \quad [30]$$

To explain the boundary conditions for particle mass concentration at the surface we consider the balance of mass flow rates near the surface in the volume element with thickness Δ_1 and length

Δ_2 along the plate surface. For a given volume element the difference between the input and output mass flow rates in the axial direction is not equal to zero due to the sliding friction of particles against the plate surface. The total mass flow rate in the axial direction can be balanced by the convectional and diffusion particle transfers in the transversal direction. But, as the convectional transfer in the transversal direction is negligible due to the insignificance of the transversal particle velocity component near the surfae, we only take into account the diffusion transfer. Thus, we may write the boundary condition for the particle mass concentration as follows:

$$\left.\frac{D_{si}}{\nu}\frac{\partial\bar{\alpha}_i}{\partial\eta}\right|_w = \bar{\alpha}_i f(x). \tag{31}$$

The expression for function $f(x)$ in the new coordinates is written as follows:

$$f(x) = C_1 \cdot x\left(\sqrt{1+\frac{\Delta_2}{x}}\,\bar{U}'_{si} - \bar{U}_{si}\right). \tag{32}$$

During the interaction of a particle with the surface it loses velocity. This velocity loss is determined as $\bar{U}'_{si} = \bar{U}_{si}[(5+2k_t)/7]$ according to Babukha & Shraiber (1972). We calculate the velocity loss on the length Δ_2. The coefficient C_1 in [32] equals a ratio of Δ_1 and Δ_2. We assume in the calculations that $\Delta_1 = \Delta\eta$ and $\Delta_2 = \Delta x$, where $\Delta\eta$ and Δx are the calculation steps in the transversal and streamwise directions, respectively. So we may write that $C_1 = \Delta\eta/\Delta x$.

In the outer part of the boundary layer the streamwise velocity component of the particles and particle mass concentration of different fractions are set equal to those in the free stream

$$\bar{U}_{si}|_\infty = 1, \tag{33}$$

$$(\bar{\alpha}_1 = \bar{\alpha}_3)|_\infty = 0.2, \quad \bar{\alpha}_2|_\infty = 0.6. \tag{34}$$

The gradient type of boundary conditions are set similar to those of the gaseous phase for the transversal velocity component and particle angular velocity in the outer part of the layer. But, unlike gas, we equal the velocity gradient to the constant, which in turn may be determined as a streamline inclination in the outer part of the layer towards the particle velocity direction of the free stream. Thus, we suggest the existence of some definite particle flow rate coming from the free stream into the boundary layer. This constant does not depend on particle size. The boundary conditions for both the transversal and angular particle velocities in that case can be written:

$$\left.\frac{\partial\bar{V}_{si}}{\partial\eta}\right|_\infty = \left.\frac{\partial\bar{\omega}_{si}}{\partial\eta}\right|_\infty = -C_2. \tag{35}$$

The constant C_2 is computed from good agreement with the experimental data and according to our investigations $C_2 = 0.1$ for all experiments.

Equations [12]–[17], with [18]–[21] and boundary conditions [22]–[27], [30], [31], [33]–[35], are numerically calculated by the tridiagonal algorithm using the six-point formula for the numerical scheme. Linearization of a non-linear terms on the left-hand side of the transport equation is carried out by Newton's method (Anderson *et al.* 1990) and for the approximation of the derivatives in the transversal direction the upwind differences were used (Roache 1980).

3.4. Pseudoviscosity coefficients

For the definition of the pseudoviscosity coefficients D_{si}, v^i_{si} let us start by considering binary particle collision with using the formulae from Chapman & Cowling (1960). Let the principle diameter be δ_1, δ_2, particle masses m_1, m_2, their inertia moments I_1, I_2 and the linear velocity V_1, V_2 and angular velocities ω_1, ω_2, respectively. Then, according to Chapman & Cowling (1960), taking into account the restitution coefficient k'_n for the normal velocity component and the friction coefficient k'_t for the tangential velocity component of colliding particles introduced by Babukha & Shraiber (1972), the velocity differences after and before collision can be calculated:

$$V'_1 - V_1 = \gamma_{21}\left\{(1-k'_n)[\mathbf{e}\cdot(V_2-V_1)]\mathbf{e} + \frac{(1-k'_t)\zeta}{(1+\zeta)}\left[\mathbf{e}\times(V_2-V_1) - \frac{(\delta_1\omega_1+\delta_2\omega_2)}{2}\right]\times\mathbf{e}\right\}, \tag{36}$$

$$V'_2 - V_2 = \gamma_{12}\left\{(1-k'_n)[\mathbf{e}\cdot(V_2-V_1)]\mathbf{e} + \frac{(1-k'_t)\zeta}{(1+\zeta)}\left[\mathbf{e}\times(V_2-V_1) - \frac{(\delta_1\omega_1+\delta_2\omega_2)}{2}\right]\times\mathbf{e}\right\}, \tag{37}$$

$$\omega_1' - \omega_1 = \frac{\gamma_{21}(k_1' - 1)}{(1+\zeta)} \left\{ \frac{2}{\delta_1} \mathbf{e} \times (V_2 - V_1) + \omega_1 + \frac{\delta_2}{\delta_1} \omega_2 - \left(\mathbf{e} \cdot \omega_1 + \frac{\delta_2}{\delta_1} \mathbf{e} \cdot \omega_2 \right) \mathbf{e} \right\}, \quad [38]$$

$$\omega_2' - \omega_2 = \frac{\gamma_{12}(k_1' - 1)}{(1+\zeta)} \left\{ \frac{2}{\delta_2} \mathbf{e} \times (V_2 - V_1) + \omega_2 + \frac{\delta_1}{\delta_2} \omega_2 - \left(\mathbf{e} \cdot \omega_2 + \frac{\delta_1}{\delta_2} \mathbf{e} \cdot \omega_1 \right) \mathbf{e} \right\}, \quad [39]$$

where the unit vector direction $\mathbf{e}$ is determined by the angle θ and the distance χ between the colliding particles at the moment of their collision, for the fixed angle φ according to figure 8. The linear velocities of both particles after collision are V_1', V_2' and the angular velocities of the particles after collision are ω_1', ω_2'. The relative particle mass for the first and second particles are calculated as $\psi_{12} = (m_1/m_1 + m_2)$ and $\psi_{21} = (m_2/m_1 + m_2)$, respectively. The coefficient ζ is determined as $\zeta = 4I/(m\delta^2)$ and for the spherical particles $\zeta = 0.4$.

These velocity differences can be considered as the particle velocity fluctuations. Let us write them in the coordinate system related to the first particle. For this reason let us direct the axis 0ξ along the particle velocity vector $\mathbf{V}_1$, and axis 0η normal to it in the plane of linear velocity vectors $\mathbf{V}_1$, $\mathbf{V}_2$ and the axis $0z$ normal to the plane $\xi 0\eta$, i.e. along the particle angular velocity vector (figures 8 and 9). The expressions for the velocity differences in the new coordinate system for the first and the second particles are defined by [A1]–[A6] in appendix A. By rewriting the obtained expressions within the Cartesian coordinate system, which is related to the plate, one can obtain [A7]–[A10] for the velocity differences, as presented in appendix A.

In order to determine the stress tensor components, we multiply the different fluctuating velocities of the particles [A3], [A6]–[A10], as presented in appendix A, and average the product over the two angles θ, φ and the parameter χ. Let us consider the following combinations:

$$\langle (u_{12}' - u_1)(v_{12}' - v_1) \rangle, \quad \langle (u_{12}' - u_1)^2 \rangle, \quad \langle (v_{12}' - v_1)^2 \rangle, \quad \langle (\omega_{12}' - \omega_1)(v_{12}' - v_1) \rangle,$$
$$\langle (u_{21}' - u_2)(v_{21}' - v_2) \rangle, \quad \langle (u_{12}' - u_1)^2 \rangle, \quad \langle (v_{12}' - v_1)^2 \rangle, \quad \langle (\omega_{12}' - \omega_1)(v_{12}' - v_1) \rangle.$$

For example, in one particular case the averaging procedure is as follows:

$$\langle (u_{12}' - u_2)(v_{12}' - v_1) \rangle = \frac{1}{2\pi} \frac{1}{\varphi_{21}} \frac{\int_0^{2\pi} \mathrm{d}\theta \int_0^1 \chi \, \mathrm{d}\chi \int_0^{\varphi_{21}} (u_{12}' - u_1)(v_{12}' - v_2) \, \mathrm{d}\varphi}{\int_0^1 \chi \, \mathrm{d}\chi}, \quad [40]$$

which is the same for other combinations.

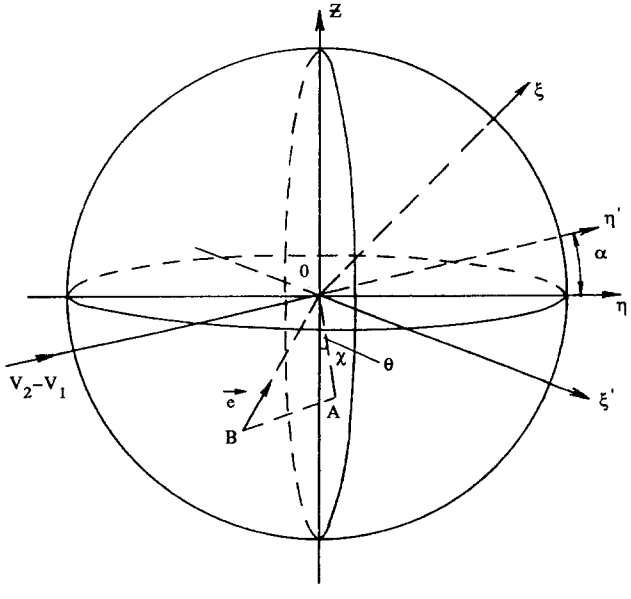

Figure 8. Schematic diagram of particle collision in space.

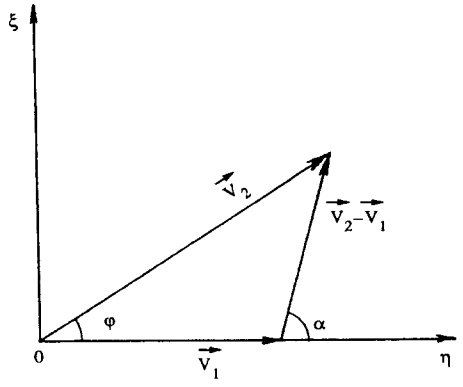

Figure 9. Schematic diagram of particle collision in plane.

The angle θ changes in the range $0 \leqslant \theta \leqslant 2\pi$ and the parameter χ, written in polar coodinates, is varied as $0 \leqslant \chi \leqslant 1$. The range of variation for the angle φ is determined from the correlation of transversal and streamwise velocity components of different particle fractions:

$$\operatorname{tg} \varphi_{21} = \operatorname{tg}(\gamma_2 - \gamma_1) = \frac{v_2 u_1 - v_1 u_2}{u_1 u_2 + v_1 v_2}. \qquad [41]$$

For the turbulent motion Babukha & Shraiber (1972) have assumed that this angle changes within $0 \leqslant \varphi \leqslant 2\pi$, which results from the suggestion that the particles approach each other with equiprobability from all directions. This approximation fails for the laminar ordered flow. Thus, we suggest that in this case the particles collide only from the windward side of their surface. The application of the averaging method to all the above written correlations gives the stress tensor components of the dispersed phase. To obtain the sought pseudoviscosity coefficients, we multiply the stress tensor components by the interparticle collision time, thus we determine this stress tensor over the volume element. The time period between collisions of two particles Δt is determined via the probability of collision as presented by Sommerfeld & Zivkovic (1992). Considering the probability of collision, which obeys a binomial distribution and which can be converted into a Poisson distribution, the authors estimate this time for the simplest case—for at least one collision. In this particular case, they assume the probability of collision is less than 0.02, when the interparticle collision time Δt is small (in their cases of mass loading 0.1–3 kg dust/kg air). Hence, by knowing this probability of collision the authors determine the interparticle collision time. For determining the probability of collision of particles Trushin & Lipatov (1963) considered the case of the ordered oncoming motion of suspended particles. The found probability is proportional to the square of the collision cross-section of colliding particles, with the diameters δ_1 and δ_2. Using the expression for the probability in the simplest case for at least one collision

$$P = \frac{\pi(\delta_1 + \delta_2)^2}{4l^2}, \qquad [42]$$

we can estimate the order of magnitude of the probability of collision. Since the average distance between the particles is an order of $l \approx (20\text{–}30)\delta$ for considered mass loading, then in our case the probability is less than 0.01. As we can see, this value is compared with that obtained by Sommerfeld & Zivcovic (1992). The obtained expression for the probability of collision is used for determining the interparticle collision time and, thus, the pseudoviscosity coefficients.

Let us define the expression for the pseudoviscosity coefficients. For this we consider the collision of a single particle of the first particle fraction (index 1) with a number of particles from the second particle fraction (index 2), and so the probability of collision can be written in this particular case according to [42] as:

$$P = \frac{\pi(\delta_1 + \delta_2)^2}{4l_2^2}, \qquad [43]$$

where the interparticle distance l_2 is taken for the second particle fraction and is calculated as $l_2 = \delta_2 \sqrt[3]{(\rho_p/\rho\alpha_2)}$. Then the interparticle collision time can be calculated according to Marble (1964) as follows:

$$\Delta t = \frac{4P}{\pi(\delta_1 + \delta_2)^2 n_2 |V_1 - V_2|}. \qquad [44]$$

n_2 is the numerical concentration of particles of the second fraction. Taking into account the above, one can obtain the pseudoviscosity coefficients, for example, for the first fraction of particles, as follows:

$$v_{s1}^1 = \langle (u'_{12} - u_1)(v'_{12} - v_1) \rangle \Delta t = \sqrt[3]{\frac{\rho_p}{\rho\alpha_2}} \frac{\delta_2 \varphi_{21} \langle (u'_{12} - u_1)(v'_{12} - v_1) \rangle}{(V_1 + V_2) E^{21}}, \qquad [45]$$

$$v_{s1}^2 = \langle (v'_{12} - v_1)^2 \rangle \Delta t = \sqrt[3]{\frac{\rho_p}{\rho\alpha_2}} \frac{\delta_2 \varphi_{21} \langle ((v'_{12} - v_1)^2 \rangle}{(V_1 + V_2) E^{21}}, \qquad [46]$$

$$v_{s1}^3 = \langle (\omega'_{12} - \omega_1)(v'_{12} - v_1) \rangle \Delta t = \sqrt[3]{\frac{\rho_p}{\rho\alpha_2}} \frac{\delta_2 \varphi_{21} \langle (\omega'_{12} - \omega_1)(v'_{12} - v_1) \rangle}{(V_1 + V_2) E^{21}}, \qquad [47]$$

$$D_{s1} = [\langle (u'_{12} - u_1)\rangle + \langle (v'_{12} - v_1)^2\rangle]\Delta t = \sqrt[3]{\frac{\rho_p}{\rho\alpha_2}} \frac{\delta_2 \varphi_{21}[\langle (u'_{12} - u_1)^2\rangle + \langle (v'_{12} - v_1)^2\rangle]}{(V_1 + V_2)E^{21}}, \quad [48]$$

where $E^{21} = \int_0^{\varphi_{21}} \sqrt{1 - k_{12}^2 \cos^2 0.5\varphi}\, d\varphi$ is the incomplete elliptic integral of the second type calculated by Byrd & Friedman (1971) with the parameter $k_{12}^2 = 4V_1 V_2/(V_2 + V_2)^2$. The upper index in the expressions of pseudoviscosity coefficients points out the corresponding transport equation where it is used. For example, index "1" refers to the equation of momentum balance of the dispersed phase in the streamwise direction, index "2" to the equation of momentum balance in the transversal direction and index "3" to the equation of angular momentum balance. The lower index in the expressions denotes the specific particle fraction. Analogously we can obtain the expressions for the second particle fraction. As mentioned above, we consider that the polydispersed phase consists of three particle fractions and thus, for these fractions the pseudoviscosity coefficients can be written as follows:

$$\nu_{si}^1 = \sqrt[3]{\frac{\rho_p}{\rho}} \frac{\cos 2\gamma_i}{2} \sum_{j=1, j\neq 1}^{3} \frac{\delta_j (V_i + V_j)}{\sqrt[3]{\alpha_i}} \{A_{ij}[\mathrm{sgn}(i-j) O_1^{ij} - O_2^{ij} \operatorname{tg} 2\gamma_i]$$

$$- sgn(i-j) C_{ij}[P_1^{ij} - P_2^{ij} \operatorname{tg} 2\gamma_i] - D_{ij}\, \mathrm{sgn}(i-j)[Q_1^{ij} - \mathrm{sgn}(i-j)(Q_2^{ij} - \varphi_{ij}) \operatorname{tg} 2\gamma_i]\}, \quad [49]$$

$$\nu_{si}^2 = \sqrt[3]{\frac{\rho_p}{\rho}} \sum_{j=1, j\neq i}^{3} \frac{\delta_j (V_i + V_j)}{2\sqrt[3]{\alpha_j}} \left\{ \frac{B_{ij} H^{ij}}{3} + \cos 2\gamma_i [A_{ij}(O_2^{ij} + \mathrm{sgn}(i-j) O_1^{ij} \operatorname{tg} 2\gamma_i) - \mathrm{sgn}(i-j) \right.$$

$$\left. \times C_{ij}(P_2^{ij} + P_1^{ij} \operatorname{tg} 2\gamma_i)] + D_{ij} \left[\frac{\varphi_{ij}}{E^{ij}} (3 + \cos 2\gamma_i) - \cos 2\gamma_i (Q_2^{ij} + \mathrm{sgn}(i-j) Q_1^{ij} \operatorname{tg} 2\gamma_i) \right] \right\}, \quad [50]$$

$$\nu_{si}^3 = \sqrt[3]{\frac{\rho_p}{\rho}} \frac{\cos \gamma_i}{6} \sum_{j=1, j\neq i}^{3} \frac{\delta_j (V_i + V_j)}{\sqrt[3]{\alpha_j}} \{F_{ij}\, \mathrm{sgn}(i-j)[R_1^{ij} - R_2^{ij} \operatorname{tg} \gamma_i] + G_{ij}[S_1^{ij} \operatorname{tg} \gamma_i$$

$$+ \mathrm{sgn}(i-j) S_2^{ij}] - 16\, \mathrm{sgn}(i-j) D_{ij}[T_1^{ij} + \mathrm{sgn}(i-j) T_2^{ij} \operatorname{tg} \gamma_i]\}, \quad [51]$$

$$D_{si} = \sqrt[3]{\frac{\rho_p}{\rho}} \frac{1}{3} \sum_{j+1, j\neq 1}^{3} \frac{\delta_j (V_i + V_j)}{\sqrt[3]{\alpha_j}} \left[B_{ij} H^{ij} + \frac{9 D_{ij} \varphi_{ij}}{E^{ij}} \right], \quad [52]$$

where the coefficients are determined as

$$a_{ij} = (1 - k'_n)\psi_{ji}, \quad b_{ij} \frac{(1 - k'_t)\zeta \psi_{ji}}{(1 + \zeta)}, \quad \psi_{ij} = \frac{m_i}{(m_j + m_j)},$$

the angle γ_i is determined via the correlation as $\operatorname{tg} \gamma_i = (v_{si}/u_{si})$, the angle φ_{ij} is determined via the correlation as

$$\varphi_{ij} = \left| \frac{v_{si}}{u_{si}} - \frac{v_{sj}}{u_{sj}} \right|,$$

the functions are determined as

$$A_{ij} = \left(\frac{a_{ij} + b_{ij}}{2} \right)^2, \quad B_{ij} = A_{ij} + a_{ij}^2 + b_{ij}^2, \quad C_{ij} = \frac{2}{15}(2a_{ij} + 3b_{ij}) b_{ij} \left(\frac{\delta_i \omega_i + \delta_j \omega_j}{V_i + V_j} \right),$$

$$D_{ij} = \frac{b_{ij}^2}{16} \left(\frac{\delta_i \omega_i + \delta_j \omega_j}{V_i + V_j} \right)^2, \quad F_{ij} = (a_{ij} - b_{ij}) b_{ij}, \quad G_{ij} = \frac{5}{16}(5a_{ij} + 7b_{ij}) b_{ij} \left(\frac{\delta_i \omega_i + \delta_j \omega_j}{V_i + V_j} \right)$$

and the total velocity is $V_i = \sqrt{u_{si}^2 + v_{si}^2}$ and $V_i = \sqrt{u_{sj}^2 + v_{sj}^2}$, $i = 1, 3$. The formulae for incomplete elliptic integrals of the first and second type K^{ij}, E^{ij} are presented in appendix B. The function H^{ij}, O_1^{ij}, O_2^{ij}, P_1^{ij}, P_2^{ij}, Q_1^{ij}, Q_2^{ij}, R_1^{ij}, R_2^{ij}, S_1^{ij}, S_2^{ij}, T_1^{ij}, T_2^{ij} are the functions of the total velocity V_i and V_j, and the angle φ_{ij}. All of these are defined by [B1]–[13] in appendix B.

Expansion of the expressions in terms of the Taylor series for small angles $\varphi_{ij} \ll 1$ gives the following pseudoviscosity coefficients, which are in the self-similar coordinates (in the non-dimensional form):

$$\frac{\nu_{si}^1}{\nu} = \sqrt[3]{\frac{\rho_p}{\rho}} \frac{\cos 2\bar{\gamma}_i}{2} \sum_{j=1, j\neq i}^{3} \frac{\mathrm{Re}_j(\bar{V}_i + \bar{V}_j)}{\sqrt[3]{\bar{\alpha}_j}} \left[-\frac{\bar{A}_{ij}}{E_{ij}}(\bar{H}_{ij} - \bar{L}_{ij}) - \mathrm{sgn}(i-j)\bar{C}_{ij}[\bar{N}_{ij} + \bar{O}_{ij} \operatorname{tg} 2\bar{\gamma}_i] \right.$$

$$\left. - \frac{\bar{D}_{ij}}{\bar{E}_{ij}} \mathrm{sgn}(i-j)[\bar{P}_{ij} - \mathrm{sgn}(i-j)(\bar{Q}_{ij} - \operatorname{tg} 2\bar{\gamma}_i)] \right]. \quad [53]$$

$$\frac{\nu_{si}^2}{\nu} = \sqrt[3]{\frac{\rho_p}{\rho}} \frac{1}{2} \sum_{j=1, j\neq i}^{3} \frac{\mathrm{Re}_j(\bar{V}_i + \bar{V}_j)}{\sqrt[3]{\bar{\alpha}_j}} \left\{ \frac{\bar{B}_{ij}}{3} - \frac{\bar{A}_{ij} \cos 2\gamma_i}{E_{ij}}(1 - \bar{k}_{ij}^2 + \bar{H}_{ij}\bar{M}_{ij}) \right.$$

$$\left. - \mathrm{sgn}(i-j)\bar{C}_{ij} \cos 2\bar{\gamma}_i(\bar{O}_{ij} - \bar{N}_{ij} \operatorname{tg} 2\bar{\gamma}_i) + \frac{\bar{D}_{ij}}{E_{ij}}[3 + \cos 2\bar{\gamma}_i(1 - \bar{Q}_{ij} - \mathrm{sgn}(i-j))\bar{P}_{ij} \operatorname{tg} 2\bar{\gamma}_i] \right\}, \quad [54]$$

$$\frac{\nu_{si}^3}{\nu} = \sqrt[3]{\frac{\rho_p}{\rho}} \frac{\cos \bar{\gamma}_i}{6} \sum_{j=1, j\neq i}^{3} \frac{\mathrm{Re}_j(\bar{V}_i + \bar{V}_j)}{\sqrt[3]{\bar{\alpha}_j}} [-\bar{F}_{ij}\bar{R}_{ij} + \bar{G}_{ij}\bar{S}_{ij} - 16\bar{D}_{ij}\bar{T}_{ij} \mathrm{sgn}(i-j)]. \quad [55]$$

$$\frac{D_{si}}{\nu} = \sqrt[3]{\frac{\rho_p}{\rho}} \frac{1}{3} \sum_{j=1, j\neq i}^{3} \frac{\mathrm{Re}_j(\bar{V}_i + \bar{V}_j)}{\sqrt[3]{\bar{\alpha}_j}} \left[\bar{B}_{ij}\bar{E}_{ij} + \frac{9\bar{D}_{ij}}{\bar{E}_{ij}} \right], \quad [56]$$

where the coefficients $a_{ij}, b_{ij}, \psi_{ij}$ are the same.

The coefficients A_{ij}, B_{ij}, F_{ij} and the functions $\bar{C}_{ij}, \bar{D}_{ij}, \bar{G}_{ij}$ depend on the angle $\bar{\gamma}_i$, which varies according to the correlation $\operatorname{tg} \bar{\gamma}_i = \bar{V}_{si}/\bar{U}_{si}$, and the angle $\bar{\varphi}_{ij}$, which varies according to the correlation

$$\bar{\varphi}_{ij} = \left| \frac{\bar{V}_{si}}{\bar{U}_{si}} - \frac{\bar{V}_{sj}}{\bar{U}_{sj}} \right|.$$

The functions are:

$$\bar{C}_{ij} = \frac{4(2a_{ij} + 3b_{ij})b_{ij}}{15} \left(\frac{\bar{\omega}_i + \bar{\omega}_j}{\bar{V}_i + \bar{V}_j} \right), \quad \bar{D}_{ij} = b_{ij}^2 \left(\frac{\bar{\omega}_i + \bar{\omega}_j}{\bar{V}_i + \bar{V}_j} \right)^2, \quad \bar{G}_{ij} = \frac{5}{8}(5a_{ij} + 7b_{ij})b_{ij} \left(\frac{\bar{\omega}_i + \bar{\omega}_j}{\bar{V}_i + \bar{V}_j} \right)$$

and the total velocity is $\bar{V}_i = \sqrt{\bar{U}_{si}^2 + \bar{V}_{si}^2}$ and $\bar{V}_j = \sqrt{\bar{U}_{sj}^2 + \bar{V}_{sj}^2}$. The functions $\bar{E}_{ij}$, $\bar{H}_{ij}$, $\bar{L}_{ij}$, $\bar{M}_{ij}$, $\bar{N}_{ij}$, $\bar{O}_{ij}$, $\bar{P}_{ij}$, $\bar{Q}_{ij}$, $\bar{R}_{ij}$, $\bar{S}_{ij}$, $\bar{T}_{ij}$, are the functions of the total velocity $\bar{V}_i$ and $\bar{V}_j$ and angle $\bar{\varphi}_{ij}$, which are defined by [C1]–[C12] in appendix C. These coefficients and functions are obtained using the transformations of the self-similar coordinate system.

As one can see, the obtained pseudoviscosity coefficients are conditioned by the flow (linear and angular velocity components of colliding particles and their mass concentration), and relaxation (the particle sizes, ratio of particle material density and the density of the carrier fluid) and also the collision parameters (restitution coefficient of the normal velocity component and friction coefficient of the tangential velocity component of colliding particles). One can see that the pseudoviscosity coefficients generally consist of three terms which describe three correlations: the correlations of linear–linear, linear–angular and angular–angular particle velocities. By means of this the peculiarities of the motion of particles in two-phase boundary layers are described. As the calculations show, the values of the pseudoviscosity coefficients vary due to the value of the pseudoviscosity coefficient of dispersed phase, which is a factor of 10^3–10^4 greater than that obtained according to the formula of Einstein $\nu_s = 2.5\beta\nu$ (Soo 1971) for a small volumetric concentration of particles ($\beta \ll 1$), for the values close to the coefficient of laminar viscosity ν of the carrier flow. While using the Einstein formula for calculating the pseudoviscosity coefficients, the numerical distribution of particle mass concentration will slightly differ from those obtained by Soo (1971), Osyptsov (1980) and Asmolov (1992). This contradicts our experimental concentration profiles. While using the given interparticle collison model, the influence of the diffusion processes and hence the pseudoviscosity coefficients on the mass and momentum transfer intensifies. This provides a satisfactory agreement with the experimental data.

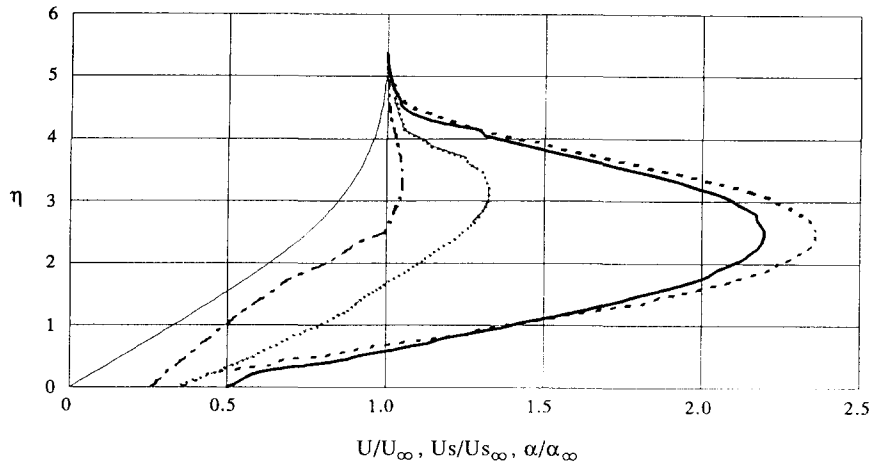

Figure 10. Numerical profiles of the axial velocity component of gas and solid phases (——, U/U_∞ $U_s/U_{s\infty}$, $X = 100$ mm, $\delta = 12\ \mu$m) and particle mass concentration α/α_∞: ——, $X = 100$ mm, $\delta = 12\ \mu$m, ----, $X = 170$ mm, $\delta = 12\ \mu$m, ·····, $X = 100$ mm, $\delta = 23\ \mu$m; – – – –, $X = 100$ mm, $\delta = 32\ \mu$m. The stream flow velocity $U_\infty = 1.5$ m/s.

4. RESULTS AND DISCUSSION

Figures 10 and 11 represent the numerical distributions of the streamwise velocity components of the gaseous and the dispersed phases and relative particle mass concentration expressed in self-similar coordinates for the cross-sections of 100 and 170 mm. Comparison of our experimental and theoretical results with calculations of other models (Soo 1971; Osyptsov 1980; Asmolov 1992) is presented in figure 12.

As one can see from figures 10 and 11, the numerical distribution of relative particle mass concentration in the laminar boundary layer is substantially non-uniform. The concentration grows monotonously from the outer part of the boundary layer, reaches its maximum at some distance from the surface and decreases towards the wall up to 20% of its value in the free stream. The growth of particle mass concentration in the outer part of the boundary layer can be explained by the penetration of inertia particles inside the boundary layer where the particles slow down. The following reduction of mass concentration towards the surface can probably be explained by the diffusion mechanism imposed by the interparticle collision and by their collisions with the surface. The prevalence of diffusion transfer over the convective transfer near the surface is connected, first,

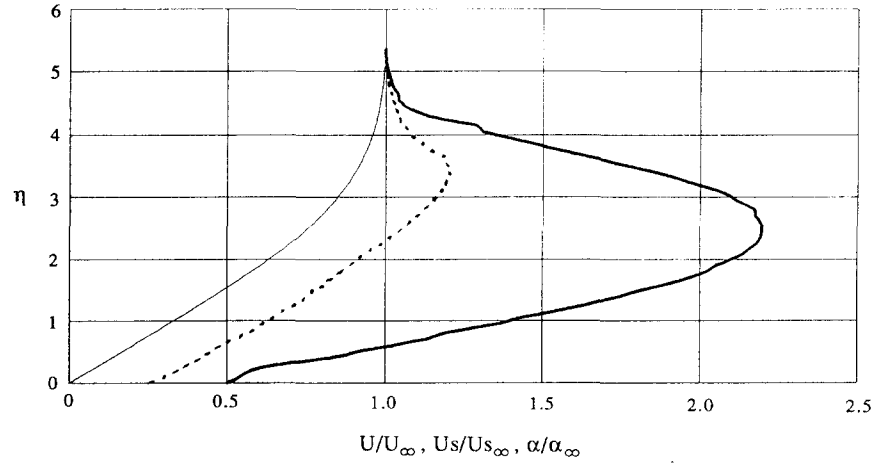

Figure 11. Numerical profiles of the axial velocity component of gas and solid phases (——, U/U_∞ $U_s/U_{s\infty}$, $U_\infty = 1.5$ m/s) and particle mass concentration α/α_∞ for $\delta = 12\ \mu$m in cross-section $X = 100$ mm for various stream flow velocities: ——, $U_\infty = 1.5$ m/s; -----, $U_\infty = 3$ m/s.

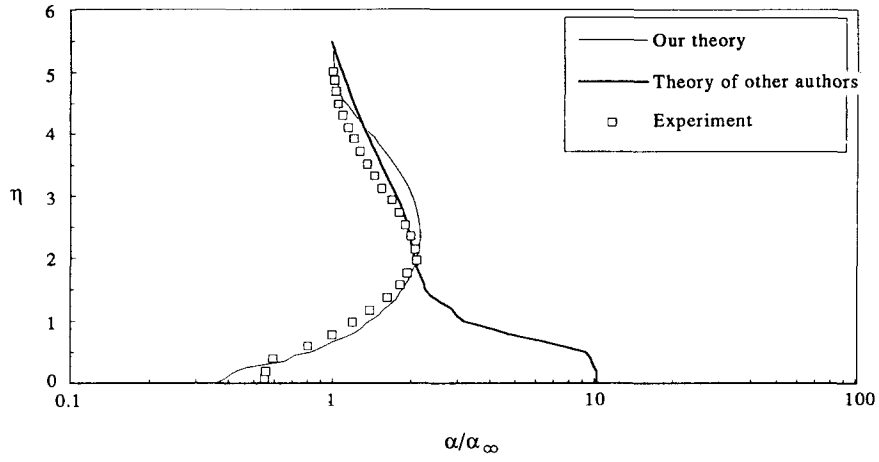

Figure 12. Comparison of experimental and numerical profiles of particle mass concentration with different models. The stream flow velocity $U_x = 1.5$ m/s and particle average diameter $\delta = 12\,\mu$m in cross-section $X = 170$ mm.

with the decrease of convective transfer near the surface, and second, with the intensification of the diffusion processes. This intensification emanates from the increase of particle velocity disturbance originated both from their interaction with the surface and from the different influence of the drag force and two lift forces, those of Magnus and Saffman, imposed on the particles of different sizes.

According to the numerical investigations, the distribution of particle mass concentration has its maximum value for fine particles (figure 10, $\delta = 12\,\mu$m). The maximum mass concentration decreases with the growth of particle size and the profile becomes less non-uniform (figure 10, $\delta = 23$ and $32\,\mu$m). It also follows from this figure that the concentration maximum shifts towards the outer part of the boundary layer for large particles. The influence of increasing free stream velocity on the concentration distribution is analogous to the influence of the growth of particle size, as is shown in figure 11. The same tendencies of modification of the distribution of particle mass concentration have been observed in the experiments.

The existing modes of two-phase laminar boundary layer on a flat plate (Soo 1971; Osyptsov 1980; Asmolov 1992), based on the description of the dispersed phase within the ideal gas conception, cannot provide the experimentally observed distributions of relative particle mass concentration (figure 12) since the mass transfer from the diffusion is not taken into account within those models. The authors calculated the two-phase laminar boundary layer with the monodispersed particles. Thus they excluded the interparticle collision mechanism from the consideration and, therefore, the diffusion transfer.

Presenting the dispersed phase within the concept of Newtonian fluid, by introducing the pseudoviscosity coefficients and specifying the boundary conditions for the dispersed phase, one can obtain the distributions of particle mass concentration by numerical calculations, which agree with our experimental data. The given model also describes the tendency of variation of the particle mass concentration with the parameters of free stream. Thus, the pseudodiffusion coefficient [56] increases with the growth of particle size or free stream velocity which leads to more uniform distribution of particle mass concentration.

Some discrepancy in the experimental and numerical results is due to the approximate description of the composition of the polydispersed admixture and the boundary conditions on the surface, specifically, when the inpenetrability condition on the surface is set in the form [30] (the particle collision with the surface is implied to be elastic).

Thus, the model shows the principle possibility for applying the pseudoviscosity approach for the description of the motion and distribution of solid admixture in two-phase laminar boundary layer developed on the flow past the unyawed flat plate.

5. CONCLUSIONS

The distributions of solid admixture in the particle-laden laminar boundary layer on a flat plate for the Reynolds numbers of flow past $Re_x \approx 10^4$ have been experimentally obtained. The profiles of particle mass concentration essentially and systematically differ from those obtained by up-to-date theoretical models. The presented mathematical model based on the approximation of the dispersed phase within the Newtonian viscous fluid, taking into consideration the introduced pseudoviscosity coefficients, was elaborated for describing the experimental results. The dispersed phase is considered as polydispersed with finite number of particle fractions that permit determination of the pseudoviscosity coefficients by the interparticle collision mechanism. The given model and specific boundary conditions, with the assumption of particle mass flux input into the boundary layer from undisturbed free stream flow and the diffusion of particles from the surface inside the boundary layer due to the collisions with the surface allow us to correctly describe the experimental data. The discrepancy between theoretical and experimental results probably comes from using both the simplest version of the model, where the dispersed phase is retricted because only three fractions of particles and the boundary conditions are set for the elastic collisions of particles with the surface.

Acknowledgements—The theoretical part of this work was supported by a Grant of the International Science Foundation No. LG 6000. The authors are grateful to Mrs H. Käbi for correcting the English.

REFERENCES

Anderson, D. A., Tannehill, J. C. & Pletcher, R. H. 1990 *Computational Fluid Mechanics and Heat Transfer*, Vols 1 & 2. Mir, Moscow (in Russian).

Asmolov, E. S. 1992 Particulate movement in the laminar boundary layer on a flat plate. *Izv. Akad. Nauk SSSR Mekh. Zhidk, Gasa* **1,** 66–73 (in Russian).

Babukha, G. L. & Shraiber, A. A. 1972 *Interaction of Particles of Polydispersive Material in Two phase Flows*. Naukova Dumka, Kiev (in Russian).

Byrd, P. F. & Friedman, M. D. 1971 *Handbook of Elliptic Integrals for Engineers and Scientists*. Springer, New York.

Chapman, S. & Cowling, T. G. 1960 *The Mathematical Theory of Non-uniform Gases*. Inostrannaja Literatura, Moscow (in Russian).

Kravtsov, M. V. 1968 Drag to the free steady motion of sphere in viscous medium. *J. Engng Phys.* **XV**, 464–470 (in Russian).

Marble, F. E. 1964 Mechanism of particle collison in the one-dimensional dynamics of gas–particle mixtures. *Phys. Fluids* **7,** 1270–1282.

Nigmatulin, R. I. 1978 *Fundamentals of Mechanics of Heterogeneous Media*. Nauka, Moscow (in Russian).

Osyptsov, A. N. 1980 Structure of a laminar disperse-mixture boundary layer on a flat plate. *Izv. Akad. Nauk SSSR Mekh. Zhidk, Gasa* **4,** 48–54 (in Russian).

Roache, P. J. 1980 *Computational Fluid Dynamics*. Mir, Moscow (in Russian).

Rubinow, S. I. & Keller, J. B. 1961 The transverse force on a spinning sphere moving in a viscous fluid. *J. Fluid Mech.* **11,** 447–459.

Saffman, P. G. 1965 The lift on a small sphere in a shear flow. *J. Fluid Mech.* **22,** 385–400.

Schlichting, G. 1974 *Theory of Boundary Layer*. Nauka, Moscow (in Russian).

Shraiber, A. A., Miliyutin, V. N. & Yatsenko, V. P. 1980 *Hydromechanics of Two-component Flows with Solid Polydispersive Substance*. Nukova Dumka, Kiev (in Russian).

Soo, S. L. 1971 *Fluid Dynamics of Multiphase Systems*. Mir, Moscow (in Russian).

Tennekes, H. & Lumley, J. L. 1972 *A First Course in Turbulence*. MIT Press, Cambridge, MA.

Trushin, G. I. & Lipatov, N. N. 1963 The probability of collision of the suspended particles in their oriented motion. *Izv. Vizshich Uchebnich Zavedeniy. Pischevaya Technol.* **5,** 110–114 (in Russian).

APPENDIX A

The expressions of the velocity differences for the first particle:

$$V'_{12\xi} - V_{1\xi} = a_{12}\sqrt{1-\chi^2}[\sqrt{1-\chi^2}(V_2\cos\varphi - V_1) - \chi V_2 \sin\varphi \sin\theta]$$
$$+ b_{12}\chi[\chi(V_2\cos\varphi - V_1) + \sqrt{1-\chi^2}V_2\sin\varphi\sin\theta] - c_{12}[\sqrt{1-\chi^2}\sin\alpha + \chi\cos\alpha\sin\theta]. \quad [A1]$$

$$V'_{12\eta} - V_{1\eta} = a_{12}\sqrt{1-\chi^2}[\sqrt{1-\chi^2}V_2\sin\varphi + \chi\sin\theta\,(V_2\cos\varphi - V_1)]$$
$$+ b_{12}\chi[\chi V_2\sin\varphi - \sqrt{1-\chi^2}(V_2\cos\varphi - V_1)\sin\theta] + c_{12}[\sqrt{1-\chi^2}\cos\alpha - \chi\sin\alpha\sin\theta], \quad [A2]$$

$$\omega'_{12} - \omega_1 = -\frac{b_{12}}{\zeta}\left[\left(\omega_1 + \frac{\delta_1}{\delta_1}\omega_2\right)(1-\chi^2\cos^2\theta) - \frac{2}{\delta_1}\chi\sin\theta\sqrt{V_1^2+V_2^2-2V_1V_2\cos\varphi}\right] \quad [A3]$$

and for the second particle:

$$V'_{21\xi} - V_{2\xi} = a_{21}\sqrt{1-\chi^2}[\sqrt{1-\chi^2}(V_1\cos\varphi - V_2) - \chi V_1\sin\varphi\sin\theta]$$
$$+ b_{21}\chi[\chi(V_1\cos\varphi - V_2) - \sqrt{1-\chi^2}V_1\sin\varphi\sin\theta] + c_{21}[\sqrt{1-\chi^2}\sin\alpha + \chi\cos\alpha\sin\theta] \quad [A4],$$

$$V'_{21\eta} - V_{2\eta} = a_{21}\sqrt{1-\chi^2}[\sqrt{1-\chi^2}V_1\sin\varphi - \chi\sin\theta(V_1\cos\varphi - V_2)]$$
$$+ b_{21}\chi[\chi V_1\sin\varphi + \sqrt{1-\chi^2}(V_1\cos\varphi - V_2)\sin\theta] + c_{21}[\sqrt{1-\chi^2}\cos\beta - \chi\sin\beta\sin\theta], \quad [A5]$$

$$\omega'_{21} - \omega_2 = -\frac{b_{21}}{\zeta}\left[\left(\omega_2 + \frac{\delta_1}{\delta_2}\omega_1\right)(1-\chi^2\cos^2\theta) - \frac{2}{\delta_2}\chi\sin\theta\sqrt{V_1^2+V_2^2-2V_1V_2\cos\varphi}\right] \quad [A6]$$

which differ from [A1]–[A3] by the coefficients a_{ij}, b_{ij} before the square brackets and transposition of the velocities V_1, V_2.

Here the variables are:

$$\cos\alpha = \frac{(V_2\cos\varphi - V_1)}{\sqrt{V_1^2+V_2^2-2V_1V_2\cos\varphi}}, \quad \sin\alpha = \frac{V_2\sin\varphi}{\sqrt{V_1^2+V_2^2-2V_1V_2\cos\varphi}},$$

$$\cos\beta = \frac{-(V_1\cos\varphi - V_2)}{\sqrt{V_1^2+V_2^2-2V_1V_2\cos\varphi}}, \quad \sin\beta = \frac{V_1\sin\varphi}{\sqrt{V_1^2+V_2^2-2V_1V_2\cos\varphi}}$$

and coefficients are:

$$a_{12} = (1-k'_n)\psi_{21}, \quad b_{12} = \frac{(1-k'_t)\zeta\psi_{21}}{(1+\zeta)}, \quad c_{12} = \frac{(\delta_1\omega_1 + \delta_2\omega_2)b_{12}}{2},$$

$$a_{21} = (1-k'_n)\psi_{12}, \quad b_{21} = \frac{(1-k'_n)\zeta\psi_{12}}{(1+\zeta)}, \quad c_{21} = \frac{(\delta_1\omega_1 + \delta_2\omega_2)b_{21}}{2}.$$

$$u'_{12} - u_1 = a_{12}\sqrt{1-\chi^2}[\sqrt{1-\chi^2}(V_2\cos(\varphi+\gamma_1) - V_1\cos\gamma_1) - \chi\sin\theta(V_2\sin(\varphi+\gamma_1) - V_1\sin\gamma_1)]$$
$$+ b_{12}\chi[\chi(V_2\cos(\varphi+\gamma_1) - V_1\cos\gamma_1) + \sqrt{1-\chi^2}\sin\theta(V_2\sin(\varphi+\gamma_1) - V_1\sin\gamma_1)]$$
$$- c_{12}\left[\frac{\sqrt{1-\chi^2}(V_2\sin(\varphi+\gamma_1) - V_1\sin\gamma_1)}{\sqrt{V_1^2+V_2^2-2V_1V_2\cos\varphi}} + \frac{\chi\sin\theta(V_2\cos(\varphi+\gamma_1) - V_1\sin\gamma_1)}{\sqrt{V_1^2+V_2^2-2V_1V_2\cos\varphi}}\right], \quad [A7]$$

$$v'_{12} - v_1 = a_{12}\sqrt{1-\chi^2}[\sqrt{1-\chi^2}(V_2\sin(\varphi+\gamma_1) - V_1\sin\gamma_1) + \chi\sin\theta(V_2\cos(\varphi+\gamma_1)$$
$$- V_1\cos\gamma_1)] + b_{12}\chi[\chi(V_2\sin(\varphi+\gamma_1) - V_1\sin\gamma_1) + \sqrt{1-\chi^2}\sin\theta(V_2\cos$$
$$\times(\varphi+\gamma_1) - V_1\cos\gamma_1)] + c_{12}\left[\frac{\sqrt{1-\chi^2}(V_2\cos(\varphi+\gamma_1) - V_1\cos\gamma_1)}{\sqrt{V_1^2+V_2^2-2V_1V_2\cos\varphi}}\right.$$
$$\left. - \frac{\chi\sin\theta(V_2\sin(\varphi+\gamma_1) - V_1\sin\gamma_1)}{\sqrt{V_1^2+V_2^2-2V_1V_2\cos\varphi}}\right], \quad [A8]$$

$$u'_{21}-u_2=a_{21}\sqrt{1-\chi^2}[\sqrt{1-\chi^2}(V_1\cos(\varphi+\gamma_2)-V_2\cos\gamma_2)+\chi\sin\theta(V_1\sin(\varphi+\gamma_2)-V_2\sin_2\gamma_2)]$$
$$+b_{21}\chi[\chi(V_1\cos(\varphi+\gamma_2)-V_2\cos\gamma_2)-\sqrt{1-\chi^2}\sin\theta(V_1\sin(\varphi+\gamma_2)-V_2\sin\gamma_2)]$$
$$+c_{21}\left[\frac{\sqrt{1-\chi^2}(V_1\sin(\varphi+\gamma_2)-V_2\sin\gamma_2)}{\sqrt{V_1^2+V_2^2-2V_1V_2\cos\varphi}}-\frac{\chi\sin\theta(V_1\cos(\varphi+\gamma_2)-V_2\cos\gamma_2)}{\sqrt{V_1^2+V_2^2-2V_1V_2\cos\varphi}}\right], \quad [A9]$$

$$v'_{21}-v_2=a_{21}\sqrt{1-\chi^2}[\sqrt{1-\chi^2}(V_1\sin(\varphi+\gamma_2)-V_2\sin\gamma_2)-\chi\sin\theta(V_1\cos(\varphi+\gamma_2)-V_2\cos\gamma_2)]$$
$$+b_{21}\chi[\chi(V_1\sin(\varphi+\gamma_2)-V_2\sin\gamma_2)+\sqrt{1-\chi^2}\sin\theta(V_1\cos(\varphi+\gamma_2)-V_2\cos\gamma_2)]$$
$$-c_{21}\left[\frac{\sqrt{1-\chi^2}(V_1\cos(\varphi+\gamma_2)-V_2\cos\gamma_2)}{\sqrt{V_1^2+V_2^2-2V_1V_2\cos\varphi}}\right.$$
$$\left.+\frac{\chi\sin\theta(V_1\sin(\varphi+\gamma_2)-V_2\sin\gamma_2)}{\sqrt{V_1^2+V_2^2-2V_1V_2\cos\varphi}}\right], \quad [A10]$$

where the angles γ_1, γ_2 are determined from the following relations: $u_1=V_1\cos\gamma_1$, $v_1=V_1\sin\gamma_1$ and $u_2=V_2\cos\gamma_2$, $v_2=V_2\sin\gamma_2$. Formulae for the particle angular velocity fluctuations are the same as [A3] and[A6], since all transformations have occurred in the plane $\xi 0\eta$.

APPENDIX B

Some expressions used in section 3.4 are listed in this appendix:

$$H^{ij}=\left[1-\frac{k_{ij}^2}{2}\left(\frac{\sin\varphi_{ij}}{\varphi_{ij}}\right)\right]\frac{\varphi_{ij}}{E^{ij}}, \quad [B1]$$

$$O_1^{ij}=\frac{k_{ij}^2\sin^2 0.5\varphi_{ij}}{E^{ij}}\left(1-\frac{V_j}{V_i}\cos^2 0.5\varphi_{ij}\right) \quad [B2]$$

$$O_2^{ij}=\frac{k_{ij}^2}{4E^{ij}}\left[\sin\varphi_{ij}\left(1-\frac{V_j}{V_i}\cos\varphi_{ij}\right)-\varphi_{ij}\frac{V_i}{V_j}\left(1-\frac{V_j}{V_i}\frac{\sin\varphi_{ij}}{\varphi_{ij}}\right)\right], \quad [B3]$$

$$P_1^{ij}=1-\frac{2}{3}\frac{V_j}{V_i}\frac{(2-k_{ij}^2)}{k_{ij}^2}+\frac{4}{3}\frac{V_j}{V_i}\frac{(1-k_{ij}^2)}{k_{ij}^2}\frac{K^{ij}}{E^{ij}}-\frac{2}{3}\frac{V_j}{V_i}\frac{\Delta^{ij}\sin\varphi_{ij}}{E^{ij}}, \quad [B4]$$

$$P_2^{ij}=\frac{4V_j(1-k_{ij}^2)}{E^{ij}V_ik_{ij}^2}\left[1-\left(\frac{1-k_{ij}^2\cos^2 0.5\varphi_{ij}}{1-k_{ij}^2}\right)^{0.5}\right]\left\{\mathrm{sgn}(V_i-V_j)-\mathrm{sgn}(i-j)\frac{\sqrt{1-k_{ij}^2}}{3}\right.$$
$$\left.\times\left[1+\left(\frac{1-k_{ij}^2\cos^2 0.5\varphi_{ij}}{1-k_{ij}^2}\right)^{0.5}+\frac{1-k_{ij}^2\cos^2 0.5\varphi_{ij}}{1-k_{ij}^2}\right]\right\}, \quad [B5]$$

$$Q_1^{ij}=\frac{2V_j}{E^{ij}V_i}\left[\sin^2 0.5\varphi_{ij}-\mathrm{sgn}(i-j)\mathrm{sgn}(V_i-V_j)\frac{\sqrt{1-k_{ij}^2}}{k_{ij}^2}\ln\left(\frac{1-k_{ij}^2\cos^2 0.5\varphi_{ij}}{1-k_{ij}^2}\right)\right], \quad [B6]$$

$$Q_2^{ij}=\frac{V_j\varphi_{ij}}{V_iE^{ij}}\left[\frac{2(1-k_{ij}^2)}{k_{ij}^2}+1+\frac{\sin\varphi_{ij}}{\varphi_{ij}}-\frac{4\sqrt{1-k_{ij}^2}}{k_{ij}^2\varphi_{ij}}\mathrm{arctg}\left(\frac{\mathrm{tg}\,0.5\varphi_{ij}}{\sqrt{1-k_{ij}^2}}\right)\right], \quad [B7]$$

$$R_1^{ij}=k_{ij}\sqrt{\frac{V_i}{V_j}}\left[1+\left(\frac{2-k_{ij}^2}{3k_{ij}^2}-\frac{2(1-k^{ij})}{3k_{ij}^2}\frac{k^{ij}}{E^{ij}}-\frac{2\Delta^{ij}\sin\varphi_{ij}}{3E^{ij}}\right)\frac{V_i}{V_j}\right], \quad [B8]$$

$$R_2^{ij}=\frac{4}{3}\sqrt{\frac{V_j}{V_i}}\frac{(1-k_{ij}^2)^{1.5}}{k_{ij}E^{ij}}\left[1-\left(\frac{1-k_{ij}^2\cos 0.5\varphi_{ij}}{1-k_{ij}^2}\right)^{0.5}\right]\left[1+\left(\frac{1-k_{ij}^2\cos^2 0.5\varphi_{ij}}{1-k_{ij}^2}\right)^{0.5}\right.$$
$$\left.+\frac{1-k_{ij}^2\cos 0.5\varphi_{ij}}{1-k_{ij}^2}\right], \quad [B9]$$

$$S_1^{ij} = \frac{\varphi_{ij} k_{ij}}{E^{ij}} \sqrt{\frac{V_i}{V_j}} \left(1 - \frac{V_j}{V_i} \frac{\sin \varphi_{ij}}{\varphi_{ij}}\right), \quad [B10]$$

$$S_2^{ij} = \frac{2k_{ij} \sin^2 0.5\varphi_{ij}}{E^{ij}} \sqrt{\frac{V_j}{V_i}}, \quad [B11]$$

$$T_1^{ij} = \frac{2}{k_{ij}} \sqrt{\frac{V_j}{V_i}} \left[1 - \operatorname{sgn}(i-j)\operatorname{sgn}(V_i - V_j)\sqrt{1-k_{ij}^2} \frac{K^{ij}}{E^{ij}}\right], \quad [B12]$$

$$T_2^{ij} = \frac{4}{k_{ij}} \sqrt{\frac{V_j}{V_i}} \frac{\sqrt{1-k_{ij}^2}}{E^{ij}} \left[1 - \left(\frac{1-k_{ij}^2 \cos^2 0.5\varphi_{ij}}{1-j_{ij}^2}\right)^{0.5}\right], \quad [B13]$$

where the parameter

$$k_{ij}^2 = \frac{4V_i V_j}{(V_1 + V_j)^2}$$

and the variable $\Delta^{ij} = \sqrt{1 - k_{ij}^2 \cos^2 0.5\varphi_{ij}}$ are calculated. The values of

$$K^{ij} = \int_0^{\varphi_{ji}} \frac{d\varphi}{\sqrt{1 - k_{ij}^2 \cos^2 0.5\varphi}} \quad \text{and} \quad E^{ij} = \int_0^{\varphi_{ji}} \sqrt{1 - k_{ij}^2 \cos^2 0.5\varphi}\, d\varphi$$

are the incomplete elliptic integrals of the first and second type, respectively.

APPENDIX C

Some expressions used in section 3.4 are listed in this appendix:

$$\bar{k}_{ij} = \frac{4\bar{V}_i \bar{V}_j}{(\bar{V}_i + \bar{V}_j)^2}, \quad [C1]$$

$$\bar{E}_{ij} = \sqrt{1 - \bar{k}_{ij}^2 + \frac{\bar{k}_{ij}^2 \bar{\varphi}_{ij}^2}{4}}, \quad [C2]$$

$$\bar{H}_{ij} = \bar{\varphi}_{ij} \bar{k}_{ij} \sqrt{\frac{\bar{V}_j}{\bar{V}_i}} \left[\sqrt{1 - \bar{k}_{ij}^2} \operatorname{sgn}(\bar{V}_i - \bar{V}_j) - \operatorname{sgn}(i-j)\bar{k}_{ij} \sqrt{\frac{\bar{V}_j}{\bar{V}_i} \frac{\bar{\varphi}_{ij}^2}{8}}\right], \quad [C3]$$

$$\bar{L}_{ij} = (1 - \bar{k}_{ij}^2) \operatorname{tg} 2\bar{\gamma}_i, \quad [C4]$$

$$\bar{M}_{ij} = \operatorname{tg} 2\bar{\gamma}_i - \operatorname{sgn}(i-j) \frac{\bar{\varphi}_{ij}}{2}, \quad [C5]$$

$$\bar{N}_{ij} = 1 - \frac{\bar{V}_j}{3\bar{V}_i} \frac{\bar{k}_{ij}^2 \bar{\varphi}_{ij}^2}{\bar{E}_{ij}^2}, \quad [C6]$$

$$\bar{O}_{ij} = \frac{\bar{\varphi}_{ij} \bar{V}_j}{\bar{E}_{ij}^2 \bar{V}_i} \left[\sqrt{1 - \bar{k}_{ij}^2} \operatorname{sgn}(\bar{V}_i - \bar{V}_j) - \frac{\operatorname{sgn}(i-j)}{3} (1 - \bar{k}_{ij}^2 + \bar{E}_{ij} \sqrt{1 - \bar{k}_{ij}^2} + \bar{E}_{ij}^2)\right], \quad [C7]$$

$$\bar{P}_{ij} = \frac{\bar{\varphi}_{ij} \bar{V}_j}{\bar{V}_i} \left[1 - \frac{\sqrt{1 - \bar{k}_{ij}^2}}{\bar{E}_{ij}^2} \operatorname{sgn}(i-j)\operatorname{sgn}(\bar{V}_i - \bar{V}_j)\right], \quad [C8]$$

$$\bar{Q}_{ij} = \frac{\bar{V}_j}{2\bar{V}_i} \frac{\bar{\varphi}_{ij}^2}{\bar{E}_{ij}^2}, \quad [C9]$$

$$\bar{R}_{ij} = 2\sqrt{1 - \bar{k}_{ij}^2} \operatorname{sgn}(\bar{V}_i - \bar{V}_j) - \operatorname{sgn}(i-j) \frac{\bar{k}_{ij}^2 \bar{\varphi}_{ij}^2}{6\bar{E}_{ij}^2} \sqrt{\frac{\bar{V}_j}{\bar{V}_i}} + \frac{\operatorname{tg} \gamma_i}{3} \bar{k}_{ij} \bar{\varphi}_{ij} \sqrt{\frac{\bar{V}_j}{\bar{V}_i}} (1 - \bar{k}_{ij}^2 + \sqrt{1 - \bar{k}_{ij}^2} \bar{E}_{ij} + \bar{E}_{ij}^2), \quad [C10]$$

$$\bar{S}_{ij} = -\frac{\operatorname{sgn}(i-j)}{\bar{E}_{ij}} \left(2 \operatorname{sgn}(\bar{V}_i - \bar{V}_j) \sqrt{1 - \bar{k}_{ij}^2} \operatorname{tg} \bar{\gamma}_i - \sqrt{\frac{\bar{V}_j}{\bar{V}_i}} \bar{k}_{ij} \bar{\varphi}_{ij}\right), \quad [C11]$$

$$\bar{T}_{ij} = \frac{2\bar{V}_j}{\bar{V}_i \bar{k}_{ij}^2} \left[1 - \frac{\operatorname{sgn}(i-j)\operatorname{sgn}(\bar{V}_i - \bar{V}_j) \sqrt{1 - \bar{k}_{ij}^2} + \bar{\varphi}_{ij} \bar{k}_{ij}^2}{\bar{E}_{ij}^2}\right], \quad [C12]$$